Icarus **157**, 193–204 (2002)
doi:10.1006/icar.2001.6798, available online at http://www.idealibrary.com on IDEAL®

Morphology of HCN and CN in Comet Hale–Bopp (1995 O1)

L. M. Woodney

Lowell Observatory, 1400 W. Mars Hill Road, Flagstaff, Arizona 86001 and Department of Astronomy, University of Maryland, College Park, Maryland 20742-2421
E-mail: woodney@lowell.edu

M. F. A'Hearn

Department of Astronomy, University of Maryland, College Park, Maryland 20742-2421

David G. Schleicher

Lowell Observatory, 1400 W. Mars Hill Road, Flagstaff, Arizona 86001

Tony L. Farnham

Department of Astronomy, University of Texas at Austin, RLM 15.308, Austin, Texas 78712-1083

J. P. McMullin

National Radio Astronomy Observatory, 520 Edgemont Road, Charlottesville, Virginia 22903-2475

M. C. H. Wright

Department of Astronomy, University of California, Berkeley, California 94720

J. M. Veal and Lewis E. Snyder

Department of Astronomy, University of Illinois, 1002 W. Green Street, Urbana, Illinois 61801

Imke de Pater and J. R. Forster

Department of Astronomy, University of California, Berkeley, California 94720

Patrick Palmer

Department of Astronomy and Astrophysics, University of Chicago, Chicago, Illinois 60637

Y.-J. Kuan

Department of Earth Sciences, National Taiwan Normal University, and Academia Sinica, Institute of Astronomy and Astrophysics, Taipei, Taiwan

Wendy R. Williams

Vanderbilt University, Nashville, Tennessee 37235

Chi C. Cheung

Physics Department, Brandeis University, Waltham, Massachusetts 02454

and

Bridget R. Smith

Northern Arizona University, Flagstaff, Arizona 86011

Received April 18, 2000; revised October 22, 2001

0019-1035/02 $35.00

We compare images of Comet Hale–Bopp (1995 O1) in HCN and CN taken near perihelion (April 1, 1997) to determine the origin of CN in comets. We imaged the $J = 1 \rightarrow 0$ transition of HCN at $\lambda = 3$ mm with the BIMA Array. Data from two weeks around perihelion were summed within four phase bins based on the rotational period of the comet. This increases both the signal-to-noise ratio and the *u–v* coverage while decreasing the smearing of the spatial features. The similarly phased narrowband CN images were taken at Lowell Observatory within the same range of dates as the HCN images. We find that there is a better correlation between HCN and CN than between HCN and the optically dominant dust. If the CN in jets does have a dust source it would have to have a very low albedo and/or small particle size. The production rates are consistent with HCN being a primary parent of CN, although there are discrepancies between the HCN destruction scalelength and the CN production scalelength which we discuss.

Key Words: **comets; Hale–Bopp; photochemistry; radio observations; data reduction techniques.**

1. INTRODUCTION

The source of the CN in comets has long been a mystery. Since the announcement of the detection of HCN in Comet Kohoutek (C/1973 E1; Huebner *et al*. 1974) and confirming detection in 1P/Halley (Despois *et al*. 1986, Schloerb *et al*. 1986, Bockelée-Morvan *et al*. 1987, Winnberg *et al*. 1987), HCN has been the most frequently suggested parent for CN. Its photodissociative branching ratio, in which 97% of HCN becomes H + CN, appears to make this species the obvious candidate (Huebner *et al*. 1992). However, there have been several challenges to the claim that HCN really fulfills all of the requirements for the CN parent. There have been several sources for CN suggested in addition to HCN, but so far none of these possibilities has given the complete answer. The source for CN must(1) be able to produce the highly collimated jets observed in some comets, (2) be consistent with the observed CN parent scalelength, and (3) have a production rate consistent with the observed CN production.

CN jets were first observed in 1P/Halley (A'Hearn *et al*. 1986). At the time it was unclear whether a gaseous source would diffuse too quickly to produce such jets, and so a dust or CHON particle source was suggested. The CHON grains are composed primarily of carbon, hydrogen, oxygen, and nitrogen and have little to no silicate component. They were first discovered in comets by the mass spectrometer experiments that flew on the Giotto and Vega spacecraft and were found to be very small (on the order of 10^{-16} g) (Kissel *et al*. 1986a,b). This small size means that most of these particles are not observed in optical reflected sunlight. For the CHON particles to produce a radical such as CN, the CN would have to directly photodissociate from molecules on the surface of the grain, photo-sputter off the surface, or have a parent which vaporizes from the grain and has an extremely short lifetime ($\tau < 1000$ s; A'Hearn *et al*. 1986, Combi 1987).

Modeling subsequent to the discovery of CN jets showed that a gaseous source such as HCN could produce the collimation of the observed features (Combi 1987). Combi's Monte Carlo modeling showed that a parent gas jet cone would expand at a slowly increasing rate within the collision zone. Then once the gas had reached the free-flow region the diffusion rate would increase rapidly, approaching a constant value. Typical half cone angles of the jets (25–30°) were found to be consistent with those observed in P/Halley (Combi 1987). A gaseous source, however, could not explain the observed radial profiles of CN along the jets. Klavetter and A'Hearn (1994) showed that although the diffuse component of CN was consistent with production from photodissociation from a gas parent, the jet component of CN required an extended source to produce its observed profile. An extended source is a source other than the nucleus or a gas parent. The behavior seen by Klavetter and A'Hearn (1994) in P/Halley may not occur in all comets, however. Boehnhardt and Birkle (1994) believed that the CN jets in P/Swift–Tuttle were consistent with their having an entirely gaseous source.

The CN parent scalelength has been fit from the CN radial profiles in many comets (cf. Combi and Delsemme 1980b, Newburn and Spinrad 1984, Randall *et al*. 1992 as quoted by A'Hearn *et al*. 1995). The value fit with Haser models (Haser 1957) has varied between 1.2×10^4 and 2.2×10^4 km at a heliocentric distance of 1 AU. Bockelée-Morvan and Crovisier (1985) pointed out that these values appear to fall short of the theoretical HCN scalelength and suggested that either C_2N_2 or HC_3N has a more appropriate scalelength for the CN parent than HCN. However, the physical relevance of scalelengths from the Haser model can be questioned.

The HCN destruction scalelength was measured in Hale–Bopp by Wright *et al*. (1998). Their measurement of 8.8×10^4 km is consistent with Crovisier's (1994) theoretical photodissociation rate for HCN of 1.5×10^{-5} s^{-1} and our measured HCN outflow velocity of 1.2 km s^{-1} (see Section 3.3). Although the CN-parent scalelengths measured in Hale–Bopp are longer than previously observed, there is still a large discrepancy between the HCN scalelength and the CN-parent scalelength.

The final factor to consider is whether the proposed parent species can produce the observed production rate of CN. Bockelée-Morvan *et al*. (1984), showed that the production rate of CN in Comet IRAS–Araki–Alcock (1983 H1) was higher than the sensitive upper limit for the HCN production rate. In Comets Austin (1989 X1) and Levy (1990 K1) the CN abundances were about a factor of 10 higher than the HCN abundances (Crovisier *et al*. 1993, A'Hearn *et al*. 1995). This indicates that a parent in addition to HCN is required. However, in the case of Halley, the production rates may be inconsistent since different models were used to calculate production rates, and nonsimultaneous data were compared when there was large time variability in the production rates (Schloerb *et al*. 1987). It is possible that different comets have different primary sources of CN and

that for some HCN is the primary parent, while for others it is not.

Other than HCN there are several possible molecular parent species for CN, including C_2N_2, HC_3N, and CH_3CN. Of these, C_2N_2 has not yet been discovered in a comet, and the production rates of HC_3N and CH_3CN in C/Hale–Bopp are about 10 times lower than that of HCN (Bockelée-Morvan *et al*. 2000). Though HC_3N and CH_3CN are certainly not the primary parent of CN due to the production rate constraint, it is still possible that C_2N_2 could play an important role. This molecule is difficult to observe, however, as the only observable C_2N_2 lines are fairly weak transitions in the near infrared (Bockelée-Morvan and Crovisier 1985). No upper limits constraining the C_2N_2 production rate have been published yet.

HNC was discovered in Hyakutake (C/1996 B2) and is another potential additional source for CN. It has been shown by Irvine *et al*. (1998) and Rodgers and Charnley (1998) that in a productive comet like Hale–Bopp, HNC can be primarily formed in the coma from gas-phase reactions between HCN and H. Therefore, HNC is probably not a significant nuclear source for CN in Hale–Bopp. Additionally, most of the HNC is formed sufficiently far from the nucleus (Irvine *et al*. 1998) that our measurements of the total HCN production should not be significantly affected by the loss of HCN to HNC. However, because chemical models cannot reproduce the amount of HNC seen in less active comets such as Hyakutake (Rodgers and Charnley 1998), its origin and potential role in producing CN in the coma is not yet completely understood.

Several authors have found that CN production rates are more strongly correlated with the dust than with the water production rates in many comets. In their study of 25 comets Newburn and Spinrad (1989) found a linear relation between the CN and dust production rates, but since CN was also present in comets with low dust activity, they concluded that it probably had both a gas and a dust source. More recently A'Hearn *et al*. (1995) found similar results from their photometric database of 85 comets, though the CN-to-dust production correlation did not hold up in all comets observed. The observed correlations suggest that at least some CN originates from dust grains.

HCN was imaged in Hyakutake both by Despois *et al*. (IAUC 6388, 1996) and by Lovell (1999), but it is the observations of HCN jets in comet Hale–Bopp combined with the near simultaneous CN imaging that has given us the opportunity to address all three of these issues in more detail. Imaging showing the extended structure of HCN allows us for the first time to examine the morphologies of both HCN and CN to determine whether they are consistent with the CN in jets having an HCN parent. We can also examine the overall production rates and scalelengths of each with these data sets. It is important to remember that Hale–Bopp was much more active than the comets we usually observe; therefore it has a larger collision zone and more chemistry is likely to be occurring in the coma than normal. Whatever these data reveal about the CN parent may be unique to Hale–Bopp.

2. OBSERVATIONS AND REDUCTION

We obtained data over a period of several weeks near perihelion on April 1, 1997. During this period the comet had at least three prominent jets. In the gaseous species, one of these jets produced a complete spiral which corresponded to production over several cometary rotations and indicated that the source location on the nucleus of that jet never became cold enough to turn completely off (Fig. 1). We also have images of the dust in the blue continuum (4450 Å) during this time. Since complete spirals are not easily seen in the dust, the source location of the gaseous spiral jet probably sees sunset, but perhaps remains in twilight; thus it never gets cold enough for the outgassing to completely stop although its production rate is reduced enough to no longer lift dust off the surface. We observed these structures in CN at optical wavelengths contemporaneously with HCN at radio wavelengths.

Table I lists all the observations used in this analysis. We have restricted our data set to observations from an approximately two-week period near perihelion (March 18–April 4, 1997) to minimize effects due to changes in the spatial scales and viewing aspect during the period in which data are directly

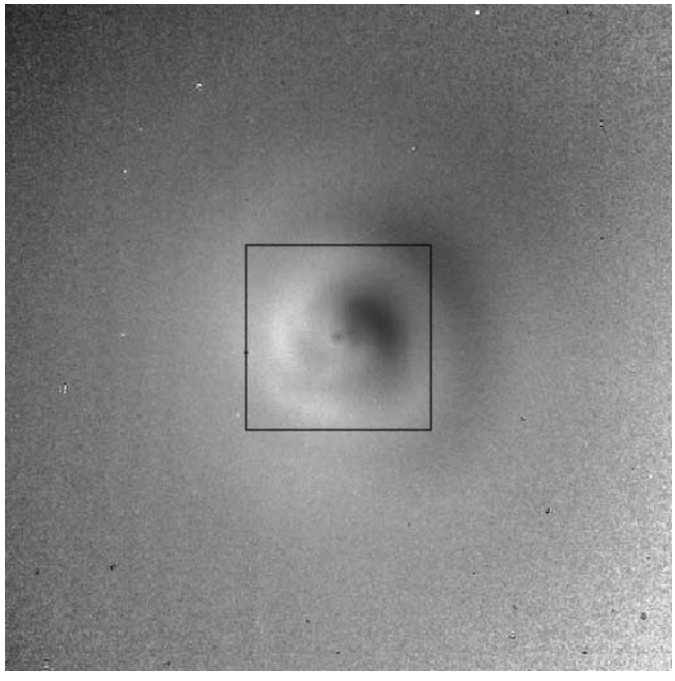

FIG. 1. This CN image from March 25 has had an azimuthal average subtracted to enhance the jets. The box is a 120 × 120″ square, representing the size of the HCN images shown in Section 3 and following. Hale–Bopp has at least three jets, which, because of the rotational pole position, the location of the jets on the nucleus, and our viewing angle, appear to overlap each other near the nucleus and are indistinguishable from each other in a single image. The overlapping jets are seen to the lower right, inside the box. One of the jets stays on throughout the cometary day, however, and can clearly be followed out in a complete spiral over nearly 700 degrees. North is to the top and east to the left in this and all other images shown.

TABLE I
CN and HCN Observations

Date (UT)	r (AU)	Δ (AU)	$PA_\odot$[a] (°)	Aspect[b] (°)	HCN (UT time)	CN (UT time)
March 18/19	0.946	1.322	353	64	12:30–01:30	
March 19	0.942	1.319	355	63	19:00–23:00	
March 25	0.922	1.319	8	54	13:30–15:15	03:06
March 27	0.918	1.325	13	51	01:30–04:00	02:54
March 28/29	0.916	1.332	15	49	20:15–04:15	02:45
March 29/30	0.915	1.338	18	47	13:30–04:30	
March 31	0.914	1.344	22	46		02:52
April 1/2	0.914	1.359	25	44	22:15–04:00	
April 3/4	0.916	1.376	31	41	14:15–04:30	

[a] Solar position angle.
[b] Angle between the pole and the line of sight for the assumed pole position of RA = 275°, Dec = −50° (Licandro *et al*. 1997).

averaged. During this time frame, the spatial scale changes by only a few percent in kilometers per pixel (the scale is 1000 km pixel^{-1} in the HCN images), so spatial smearing is a minor issue.

Our HCN images of the $J = 1 \rightarrow 0$ transition at 88.63185 GHz were made with the BIMA Array[1] at Hat Creek Observatory. The array consisted of nine 6.1-m antennas in a compact configuration, resulting in a synthesized beam size of $\approx 9''$. The data were reduced using MIRIAD (multichannel image reconstruction image analysis and display) for calibration, inversion to the image plane, and deconvolution (Sault *et al*. 1995). The velocity resolution in the data used here was 0.33 km s^{-1}. However, individual velocity planes had an insufficient signal-to-noise ratio (S/N) to give meaningful results. Therefore the images used in this analysis are integrated intensity images. They were created by summing over the $F = 2 \rightarrow 1$ and $F = 1 \rightarrow 1$ hyperfine components of the transition. The $F = 0 \rightarrow 1$ component of the $J = 1 \rightarrow 0$ transition was omitted due to a low S/N in that line. An analysis of the complete BIMA HCN data set can be found in the paper by Veal *et al*. (2000), while an examination of the simultaneous mosaics of HCN and HCO^+ together with discussion of HCN scalelengths can be found in the paper by Wright *et al*. (1998).

Comets are dynamic objects, with constantly changing morphologies. This poses a true challenge for interferometric techniques which require emission to be constant over the synthesizing period. The traditional approach to creating images is to use all of the visibility data from a day's observing to create a single image. The best u–v plane coverage, and therefore the least distortion in the image due to incomplete sampling of the u–v plane, comes from summing an entire track from rise to set of the comet. This technique also gives the best S/N in the diffuse gas emission. This diffuse component has a relatively constant morphology and is well fit by a Haser spherical outflow model, though its peak intensity changed by as much as 25% on time scales as short as 2 h (Veal *et al*. 2000). Overall, the diffuse component accounts for 80–90% of the the flux observed.

Information about the gas in jets, however, would be lost if data were summed over an entire track because this time period is comparable to the rotation period of the comet, and the jet morphology varies through a complete cycle in this time. If the data are summed over a small fraction of the rotation period, the effects of the comet's rotation are reduced, but the limited u–v coverage can distort the image. Additionally, with less integration time per image, S/N is reduced.

In Comet Hale–Bopp we can address this problem because the comet has a well-determined rotational period of 11.309 h and the morphology is consistently repeated from one rotation to the next at any one rotational phase over a several-week period near perihelion (Farnham *et al*. 1997, Jorda *et al*. 1997, Licandro *et al*. 1998). Therefore, to reduce spatial smearing of the jets, increase the signal-to-noise ratio, and increase u–v coverage at each rotational phase, we have taken all of our data over two weeks around perihelion and divided them into four rotational phase bins (Fig. 2). Zero phase is defined at perihelion: 3:18:43 UT, April 1, 1997, and our rotational phase bins are bounded by 0.00, 0.25, 0.50, and 0.75 phase. Smaller bins in the rotational phase would have been desirable but would have required more data or data with higher S/N than were available to retain the same quality of the images. The current choice represents a compromise, maximizing S/N and u–v coverage while minimizing the spatial smearing of the jets. Four rotational phase bins yielded at least 4-σ detections of the extended morphology at all phases. The data within each rotational phase bin are inverted together as if they were a single observation. Thus we create four

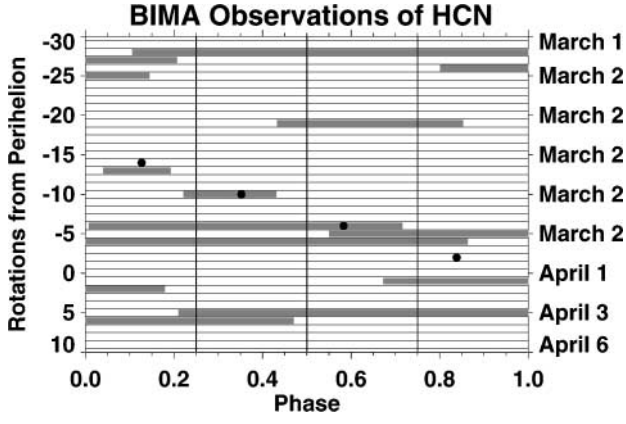

FIG. 2. The times of our CN and HCN observations. Division of the data into phase bins is shown. The shaded bars represent the HCN data, while the filled circles are the times for the CN data used in this analysis. Zero phase was set at perihelion on April 1, 1997, 3:18 UT. Bins of one-quarter rotation were chosen to maximize the signal-to-noise ratio and u–v coverage while minimizing effects from spatial smearing.

[1] The BIMA Array is operated by the Berkeley–Illinois–Maryland Association under funding from the National Science Foundation.

images, each averaged over one-quarter of the comet's rotation period.

Our CN and blue continuum dust images were taken at the Lowell Observatory 42-in. Hall telescope on Anderson Mesa. We used a blue-sensitive SITe 2K CCD in a 2 × 2 binned mode. The plate scale of the images is 1.14″ per pixel while the average seeing was 2–3″. The 19′ field of view extends far beyond the effective size of the HCN images.

To isolate the CN emission from the comet we used a narrowband filter with a FWHM of 62 Å centered on 3870 Å from the Hale–Bopp filter set. This isolates the CN $\Delta v = 0$ band of the ($B^2\Sigma^+ \rightarrow X^2\Sigma^+$) transition which is excited by solar fluorescence. Exposure times were typically 10 s. Calibration and continuum subtraction of the images was done using the method outlined by Farnham *et al.* (2000).

The dust images used both for continuum subtraction from the CN images and for comparison to the HCN and CN morphologies were also taken with a narrowband filter from the Hale–Bopp filter set. The blue continuum filter has a FWHM of 67 Å and is centered at 4450 Å. At this wavelength the dust is seen in reflected sunlight. Typical exposure times were 2–5 s. To facilitate comparison of the optical images to the binned HCN images, we have chosen representative images for both CN and dust with phases that fall near the center of each HCN phase bin (see Table I).

Many of the images throughout this paper have been enhanced so that we can see the jets in the images. The technique used here is to compute an azimuthally averaged radial profile of the image, then to turn the radial profile back into an array, and then to divide or subtract the new image from the original. The advantages to this technique are that the jet locations are not affected by the processing and the sunward/anti-sunward asymmetries also remain. The intensity of the jets relative to the original images is shown in Fig. 3. The brightest of the jets are 8–15% of the original maximum brightness and 10–30% of the original brightness at 10,000 km.

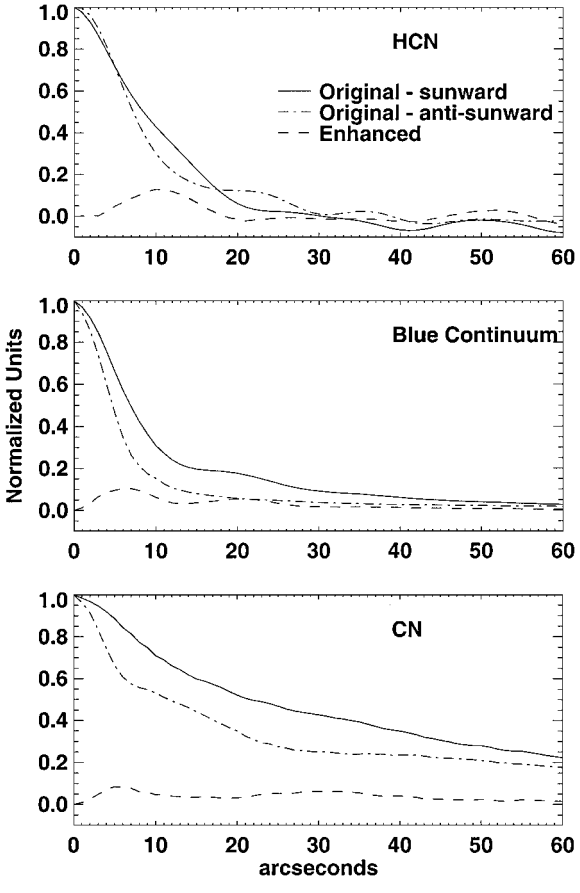

FIG. 3. The image enhancement technique used in this paper is azimuthal average subtraction. The scale of the jets relative to the original images is shown here. The peak brightness of each image was normalized to 1 before enhancement. The average radial profile is calculated and then turned into a two-dimensional image, which is subtracted from the original image. This removes the radial falloff which dominates images, leaving only the jet structure. The primary advantage of this technique is that it does not affect the location of where jets appear in the enhanced images. The plots show a radial profile from the original and the enhanced image in the sunward direction for HCN, blue continuum, and CN. An anti-sunward cut is also shown for the original images to demonstrate the differences in the asymmetry for the different species. The brightest of the jets are generally 8–15% of the original peak brightness, or 10–30% of the original brightness at the radius of the jets.

3. ANALYSIS

3.1. Observational Effects

Our two data sets give us a unique opportunity to use morphology to examine the parentage of CN. For the first time we can look at where the HCN is in the coma to determine whether it is consistent with the CN jets having an HCN parent.

There are several important differences between our two data sets which constrain how we can interpret them. Our radio images have significantly lower sptial resolution than the optical images, and features have been blurred both spatially and temporally. Additionally, the radio and optical images utilize different samplings of the u–v plane. The radio data have incomplete coverage, containing only the portion filled in by the nine antennas (36 baselines) over the time of the observations, while each optical image has essentially complete u–v coverage.

The radio images have a synthesized beam of 9–10″, while the optical images are limited by the effective seeing of 2–3″. Additionally, the optical images represent a very brief snapshot of the comet. They cover such a small fraction of the 11.3-h rotation period that there is no blurring due to motion of the gas. In contrast, the phase bins for the HCN images represent almost 3 h of time. In that time the radial outflow of the gas near the nucleus in the plane of the sky is 10–12″, as measured on optical images of CN at 40,000 to 50,000 km from the nucleus. A third factor affecting the resolution is that we have summed data at the same phase from several cycles and the orientation of the comet on the sky has changed slightly during this period. If we use the pole position fit by Licandro *et al.* (1997; RA = 275°,

Dec $= -50^\circ$) we calculate that the aspect angle, the angle between the pole and the line of sight, has changed by 21° over the course of our observations. As shown by Samarasinha (2000), a change this small in the aspect angle will have little effect on the morphology of the coma when the active regions on the surface are large, as is believed to be the case for Hale–Bopp (Samarasinha *et al*. 1997). Another geometric effect is that the solar position angle changes by 40° during the time period over which we sum data. If we were studying the tail this would result in significant smearing; however, we can tell from the optical images that this has little effect on the jets from cycle to cycle during our interval. The aspect angles and solar position angles are listed in Table I. Since the successive cycles of rotation of the primary optical gas jet are separated by $\approx 20''$ it would be reasonable to expect that any HCN jets would have similar separation and that the detection of individual jets would be at the limits of our resolution. What we see in our HCN data are the jets smoothed together by the convolving function created by the above factors.

The benefit of adding together data at the same phase from several cycles is far greater than the loss from adding additional smearing. It greatly increases the signal-to-noise ratio in the individual images and increases our u–v plane coverage. Therefore, the effects of structural artifacts caused by incomplete u–v plane coverage are greatly reduced.

Despite the increased coverage, we must still investigate the effects of u–v plane coverage on the morphology of the jets. To do so we have taken a blue continuum dust image and sampled it with the same u–v coverage as in our HCN images. We have chosen to use a dust image, rather than a CN image, because the radial profile of the dust more closely approximates the radial profile of a parent species like HCN, than does that of a daughter species like CN. This allows us to examine the effects of the u–v sampling on the large-scale structure of the HCN.

The original dust images, those from before the application of reductions to enhance jet features, were used as a model for what a comet looks like in the sky plane (Fig. 4a). First, noise was added to these images to give them a S/N similar to that found in the HCN images. Then, given the position of the comet in the sky, and the antenna baselines over the time of the observations, we calculated which spatial frequencies were sampled and created a visibility data set for the dust. Therefore, we see the dust as we would have if we had observed it with the interferometer. We used routines available in the MIRIAD package for this modeling.

Once the data were sampled, the resultant visibilities were Fourier transformed to bring the data back into the image plane. This result was cleaned in the same manner as for the HCN images. The result for phase 0.12 is shown in Fig. 4b. The central peak now sits in the familiar bowl of a structure that has had flux resolved out due to the missing short baselines. The array cannot detect flux that is smooth on scales larger than about 10 times the synthesized beamwidth because we do not have data from a zero-length baseline.

To demonstrate how u–v coverage affects our images, one dust image has been sampled with the u–v coverage for each of

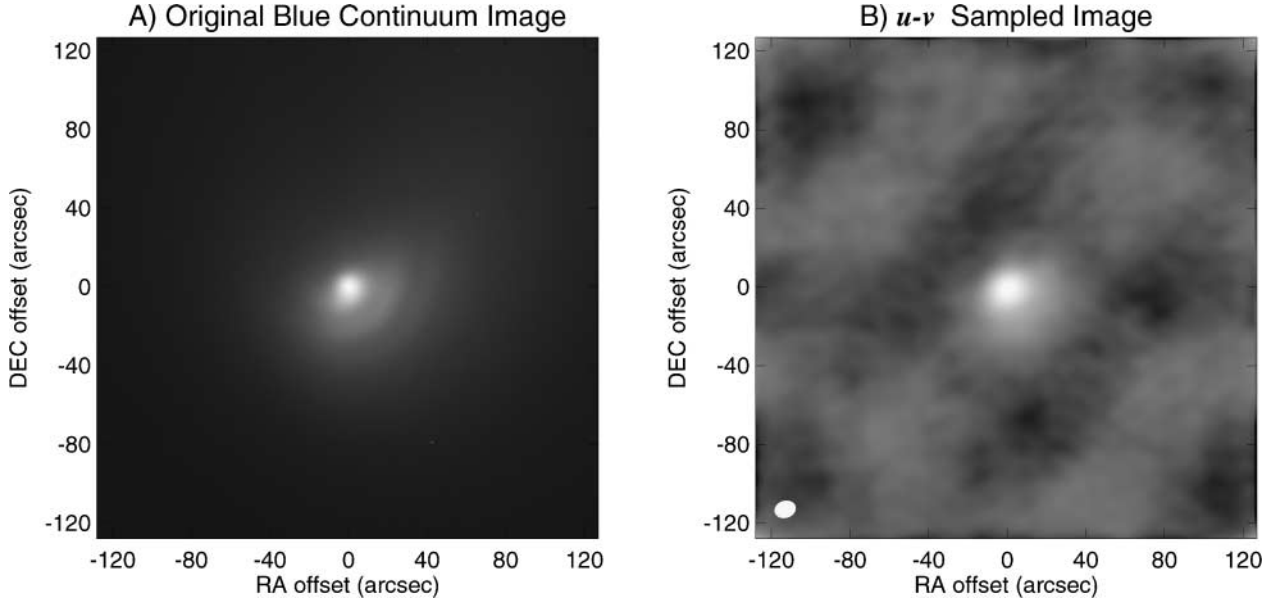

FIG. 4. A blue continuum dust image of P/Hale–Bopp at 4450 Å taken on March 25, 1997 has been sampled with the same u–v coverage contained in our phase-0.125 data. Panel A shows the original image, and panel B shows the image after it has been sampled. The beam ($10.3 \times 8.5''$) is shown in the lower left corner of the sampled image. Dust was chosen because its large-scale $1/\rho$ falloff is similar to that of a parent molecule. This shows the effects of looking at the comet with the interferometer. The ring seen around the central emission in panel B is evidence that flux has been lost due to the lack of short baselines.

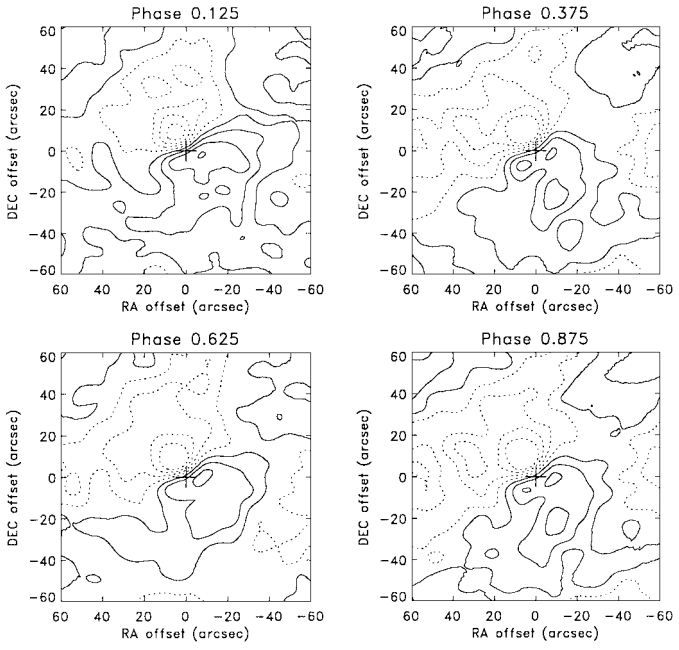

FIG. 5. A single dust image has been sampled with each of the four u–v coverages. Before sampling, the image was rescaled so that the dust jets would have spacings similar to those of the gas jets. The large-scale structure in the rescaled image remains close to the type of radial profile we would expect for HCN. An azimuthal average has been subtracted from the images to more clearly show how differing u–v coverage affects the jet structure.

the four phase bins. The results are shown in Fig. 5. This image was rescaled before the sampling was done, so that the dust jets had the same spatial scales as the optical gas jets. We again use dust for this comparison, because even with the rescaling, the large-scale structure is more similar to that of HCN than that in the CN images would be. Additionally, since the dust jets are more sharply defined than the gas jets, it is easier to see the differences in these images. To enhance the jet structure, these images are shown with an azimuthally averaged radial profile subtracted. The differences seen are the result of the variation in the synthesized beam and side lobes, caused by the unique u–v coverage in each phase bin. Since all four phase bins have good coverage, the changes are slight but clearly present.

More significant than the effects of changing u–v coverage is how the jet structure at all four phases has changed from the original optical images. Figure 6, column A shows a set of CN images, one corresponding to each bin of rotational phase, and each overlayed with its u–v sampled counterpart. To enhance the jets an azimuthal average was subtracted after the sampling from both the original images and the sampled images. The jets have been smeared together in the sampled images as expected. However, the locations of the peaks of the jet emission have also moved slightly radially outward. This is most evident at phases 0.125 and 0.625.

This radial shift is at least in part explained by the overall radial profile of the coma. Figure 6, column B shows the same data, sampled after the average radial profile was removed. In this case there is almost no radial shift. The radial shift seen in column A, as well as the corresponding radial shift which will be in the HCN data, is probably due to sampling a steeply varying function with low resolution; this is similar to the effects seen in observations of Jupiter's synchrotron radiation (Dulk *et al*. 1997, de Pater and Sault 1998). This shift must be remembered when comparing the CN to the HCN images. Despite the challenges in interpreting these data, they reveal far more about the nature of the HCN morphology than we have ever seen before.

3.2. Comparison of HCN and CN Morphology

To understand the relationship of HCN to other species in the coma, we compare it to both CN and the dust in the blue continuum at 4450 Å. Figure 7 shows CN and dust images which have been overlayed with contour maps of the HCN. All images shown here were centered on the emission peak and then azimuthally averaged radial profiles were subtracted to enhance the jets. The HCN emission peak corresponded to the JPL ephemeris position, as was calculated after the apparition (solution JPL #146). The contour intervals of the HCN overlays each represent 2-σ steps, where σ was calculated in the original images.

The morphologies of the CN and optical dust images are quite different. The dust jets are more highly collimated and spaced closer together by about a factor of 2 than the CN jets. From the motion of the jets we derive a projected outflow velocity of 1.2 km s^{-1} for the CN between the projected radial distances of 40,000 and 50,000 km, while the projected velocity of the dust is correspondingly about a factor of 2 smaller. These are lower limits for the outflow velocities at these distances. Calculation of the de-projected velocity is dependent on both the pole position and the location of the jets on the nucleus. While there are several published pole positions, we do not have sufficient information about the source location of our measured jets to calculate a meaningful de-projected velocity.

Additionally, the dust jets are seen only as arcs on the sunward side while some of the CN jets are complete spirals. When looking at the images that have not had the jet structure enhanced, the dust images show a strong sunward/anti-sunward asymmetry. CN is also asymmetric but shows significant emission on the anti-sunward side, as can be seen in the radial profiles shown in Fig. 3 (the technique used to enhance the jets in CN also enhances the sunward/anti-sunward asymmetry in the CN, so it is much more visible in Fig. 7 than in the original images). These radically different morphologies make it clear that the optically dominant dust is not the parent of CN.

In comparing the HCN images to the CN images it is important to remember that the most significant features are the ones near the center of the images where the S/N is high in the original images. The region of 3-σ or higher detection of HCN extends to a radius of about 30″ (30,000 km) from the peak of the emission. This limit is in part due to the primary beam response of the interferometer. At 60 arcseconds away from the center, the

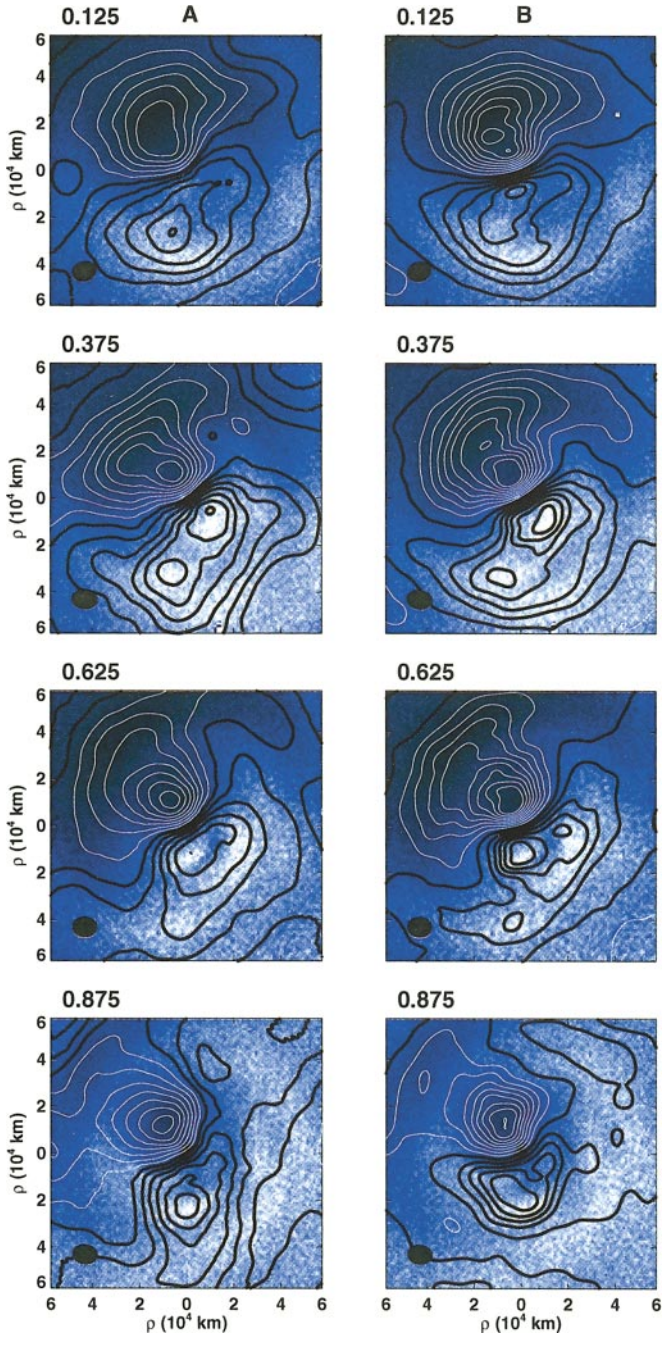

FIG. 6. A CN image from each of the four phase bins has been sampled with the same u–v coverage as the relevant HCN data set. The color images are the unsampled CN data, while the contours show the u–v sampled data. Positive contours are solid black lines and negative contours are dashed white lines. In column A, azimuthal averages were removed from the data after the sampling, while in column B the azimuthal average was removed from the CN image before sampling. This shows the effect of the steep radial falloff of the coma on the sampling. In both cases the jets have been smeared together, but in the interferometrically sampled images in column A they have shifted radially, while in column B, there is very little radial shifting of the peaks between the original and the sampled image.

intensity measured in the radio image is about half of the true intensity.

There is a better correlation in morphology between HCN and CN than between HCN and optical dust. This is seen most

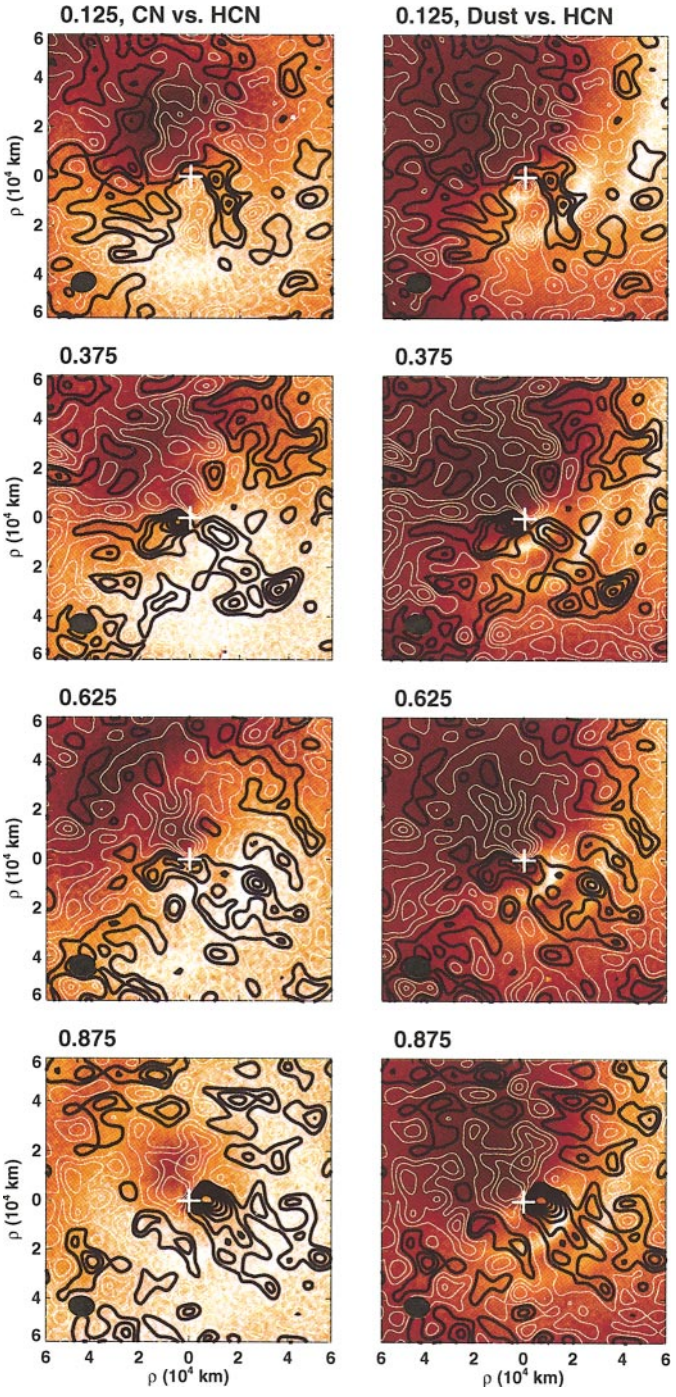

FIG. 7. A comparison of CN and optical dust to HCN in each of the four phase bins. The color images are the optical data while the contours are the radio data. Contours are drawn at 1-σ intervals ($\sigma = 0.3$ Jy) with the positive contours in black and the negative contours in white. All images have had an average radial profile subtracted to enhance the jets.

strongly in phases 0.375 and 0.625 where there is an HCN peak to the southeast. Though there are no dust jets in those locations, in each case the HCN peak lies just inside a CN jet. This is the same offset as we saw when comparing the CN images to their u–v sampled counterparts. However, the correlation between HCN and CN is certainly not perfect. There is not a strong correlation between the intensities of the two species—we do not always see HCN where the CN jets are bright. The lack of HCN jets in these regions, however, may be due to insufficient S/N for detection.

Having shown that the optically important dust is not well correlated with the gas, if there is a dust source for CN it must have some specific properties. Since a dust source of the CN jets is not observed at optical wavelengths, the dust particles must have a very low albedo and/or be small enough that they do not efficiently reflect sunlight. Very small particles may also explain how dust particles could match the high outflow velocities observed in the gas jets, because small particles could be coupled with the gas flow. The comparison of the CN and HCN morphologies indicates that though some portion of the CN in jets comes from an HCN parent, it is possible that there is a second source for CN. This is consistent with and thus provides support for the result of Klavetter and A'Hearn (1994), whose analysis of CN jets in P/Halley led them to conclude that the CN jets must have an extended source.

3.3. Scalelengths

As a test of whether HCN is the parent of CN we need to know not only about the jet morphology but whether the bulk radial distributions of HCN and CN are consistent as well. Festou *et al*. (1998) have shown that in many comets the CN formation scalelength appears to be much shorter than the HCN destruction scalelength. We have measured the scalelength for HCN and modeled a parent scalelength for CN. However, we must consider whether the model used actually provides physical information that constrains whether HCN can be the parent of CN. In the absence of a detailed 3-D model of velocity, optical depth, and chemistry, one usually uses simple parameterized models to describe radial distributions.

The simplest model is the Haser model (Haser 1957). This model describes a steady-state, spherical outflow at a constant velocity. It comes closest to simulating the conditions for a parent molecule, since in this case the velocity truly is purely radially outward and there are no excess velocities from photodissociation. The Haser model is a nonphysical model for generations beyond the parent molecule if dissociation takes place outside of the region where collisions force all species to flow radially outward. However, it is still a useful model for both parent and daughter species because spatial radial profiles can usually be empirically well fit using an appropriate pair of parent–daughter scalelengths.

A vectorial model (Festou 1981), which allows the photodissociation product fragments to have excess velocities into 4π steradians rather than being entrained radially outward, works best for fragments for which the time scale of production is much larger than $r_{\rm coll}/v$, where $r_{\rm coll}$ is the radius of the collision zone and v is the parent's velocity. When the above condition is true, there is a mathematical relation between the parent and daughter lifetimes from the vectorial model and the scalelengths of the Haser model (Combi and Delsemme 1980a). This requires a knowledge of the parent outflow velocity and the excess velocity from photodissociation of the daughter.

In Hale–Bopp the collision zone is very large. Combi *et al*. (1997) estimate that it is on the order of 2.7×10^5 km as compared to 1.9×10^4 km for a more typical Halley-type comet. These values are somewhat model dependent on the species and collisional cross- sections used in the calculations, but it is certain that the collision zone in Hale–Bopp is more than a factor of 10 larger than in typical comets. The effect of this large collision zone is that the vectorial model becomes representative of physical conditions only at much larger distances than in most comets. The standard vectorial model assumes that both the parent and daughter velocities are constant with cometocentric distance, which is not the case in Hale–Bopp since measurements of the gas outflow show that acceleration is significant out to at least 100,000 km (Schleicher *et al*. 1999). Most of the region we are interested in for the HCN–CN problem is actually in a transition zone between the pure radial outflow of a Haser model and the absence of a directional preference of the vectorial model. Collisions are frequent enough to keep the gas preferentially flowing outward, but there are still some photodissociation fragments traveling in all directions. Therefore, the Haser model may be more nearly correct for the HCN–CN problem than the vectorial model because the collisions enforce a radially outward flow. However, a Monte Carlo model of the gas outflow is required to correctly model the transition zone since it can include both collisions and acceleration.

The scalelength for the destruction of HCN in Hale–Bopp was determined by Wright *et al*. (1998) to be $8.8 \pm .9 \times 10^4$ km from mosaiced data which included both multiple pointings of the interferometer and zero-length baseline data. Snyder *et al*. (2001) derived the same scalelength from the HCN data used in our current analysis, showing that the loss of flux due to the lack of the zero-length baseline does not affect the determination of scalelengths. Both of these determinations assume that the HCN is thermalized at a constant temperature and that column density is proportional to the radio line brightness. While it is true that significant temperature changes in the innermost coma are probable (Combi *et al*. 1997), the calculations of both Snyder and Wright exclude the innermost 10,000 km and so are insensitive to any temperature changes in that regime.

For a constant outflow velocity of 1.2 km s^{-1} as fit to the data by Wright *et al*. (1998) and also consistent with the half-width of the line, the measured scalelength corresponds to a lifetime of 7.3×10^4 s. This lifetime is consistent with the theoretical prediction of the lifetime against photodissociation at solar minimum of 6.7×10^4 s (Crovisier 1994). It is known from

observations of the CN jets that the gas is accelerating out to at least 100,000 km (Schleicher *et al*. 1999). The velocity starts out at a fraction of a kilometer per second and may become as high as 3 km s^{-1} by 10^6 km (Combi *et al*. 1997). However, the outflow velocity we have assumed is not unreasonable for the average velocity of HCN from the time of release from the nucleus until photodissociation of HCN.

There are additional uncertainties in measuring the scalelength from the HCN profile due to optical depth effects, temporal fluctuations, and excitation effects. If acceleration in the innermost coma is gradual (i.e., the gas is traveling much more slowly than our assumed velocity for a significant amount of time), the lifetime could be underestimated, but if the innermost coma is optically thick to the photodissociating wavelengths, the lifetime could be overestimated. We must therefore assume some uncertainty in the lifetime as deduced from this observed scalelength. The region in which the coma is optically thick to Ly-α, the primary source of HCN photodissociation, has been estimated to have a radius of about 1000 km (Combi *et al*. 1997). Combi *et al*. also find that the gas accelerates up to 0.8 km $s,^{-1}$ a significant fraction of our assumed velocity, within 200 km of the nucleus. These results suggest small differences in the lifetime compared to the nominal value.

A Haser model has been used to fit both parent and daughter scalelengths to our azimuthally averaged wide-field CN images (D. G. Schleicher, personal communication, 1999), yielding scalelengths of $(3.5 \pm 1.0) \times 10^4$ and 4.5×10^5 km, respectively. There is some uncertainty in these scalelengths because the Haser model has a tendency to give equally good fits as one scalelength is increased while the other is decreased. The scalelengths given here are from the minimum of chi-squared.

Clearly the Haser formation scalelength of CN is much shorter than the measured destruction scalelength for HCN. However, we must ask if this actually places a constraint on HCN as the primary CN parent. In Hale–Bopp the collision zone is three times the scalelength of HCN, and eight times the fitted Haser model formation scalelength for the CN. Thus we can assume a significant fraction of the CN is formed within the collision zone where the Haser model should work reasonably well, as all molecules are forced to flow radially outward in this region. On the order of 90% is formed within the collision and transition zones, and only 10% outside is formed in the region where the vectorial model is required. This tells us that if we believe the physical situation should fall between the Haser and vectorial extremes, we should probably directly compare the measured HCN scalelengths to the Haser-fit scalelengths, which leaves us with a difference of more than a factor of 2. These results would imply that if there is any correlation between the model scalelengths and physical scalelengths, that CN requires a second parent with a scalelength about a factor of 2 shorter than that of HCN. To obtain a definitive physical formation scalelength of CN, a complete Monte Carlo model will be required. Such a model, which accounts for acceleration, collisions, and chemistry, is beyond the scope of this paper.

3.4. Production Rates

Another test for the relationship of HCN and CN in the coma is their relative production rates. Since the photodissociation branching ratio for HCN is that 97% goes to H + CN, we would expect to see approximately the same production rates in CN and HCN if HCN is the primary parent of CN.

For the CN, D. G. Schleicher (personal communication, 1999) used narrowband photometry to find a production rate (Q) for CN of $(3.2–3.6) \times 10^{28}$ molecules s^{-1} at perihelion. The largest source of error in the calculation of this production rate is the lifetime of CN. The value used here was 2.1×10^5 s, which works well with many observations but is highly uncertain. The theoretical value for the CN lifetime at solar minimum is 3.2×10^5 s (Huebner *et al*. 1992). Use of this lifetime would reduce the production rate to $(2.1–2.4) \times 10^{28}$. However, since there are no laboratory measurements of the cross section of CN to photodissociation, the theoretical lifetime of CN has a large uncertainty (Huebner *et al*. 1992). If we derive a lifetime from the Haser scalelength fit to the CN data and the gas outflow velocity derived from the HCN, then we would have a lifetime for CN of 3.75×10^5 s. This lifetime yields a production rate of $(1.8–2.0) \times 10^{28}$. There are also radio measurements of CN near perihelion, which yielded a production rate of 2.6×10^{27} (Ziurys *et al*. 1999). This is below the range of possible production rates that can be derived from the optical data and is inconsistent with the HCN production rates discussed below as it would require significantly more HCN than CN in the coma. Which of the lifetimes and therefore which set of production rates is closer to being correct for the optical CN remains unclear, but we can set the lower limit on the CN production rate near 1.8×10^{28} and the upper limit near 3.6×10^{28}.

Millimeter-wave observations yielded HCN production rates for Hale–Bopp near perihelion near 2.3×10^{28} molecules s^{-1} (Biver *et al*. 1997, Wright *et al*. 1998, Lovell 1999). A somewhat larger HCN production rate of 5.6×10^{28} molecules s^{-1} was found by Magee-Sauer *et al*. (1999) in an analysis of infrared spectra of HCN. They assumed a velocity that was higher than that implied by the model of Combi *et al*. (1997), but incorporating this velocity difference would only drop the production rate by ~5%. We can not explain this large difference in production rates for HCN.

The higher production rate of HCN is inconsistent with the CN production rates. There cannot be significantly more HCN than CN because 97% of photodissociating HCN molecules become H + CN fragments (Huebner *et al*. 1992). Some of the HCN can be lost through chemical reactions such as HCN + H → H + HNC (Rodgers and Charnley 1998). However, this effect is small in comparison to the total production rate of HCN. To obtain consistent results with the larger HCN production rate the lifetime of CN would have to be at least as short as 7.9×10^4 s. It is unlikely that the theoretical lifetime is wrong by a factor of 4 (Bockelée-Morvan and Crovisier 1985).

Given the production rate of HCN from the radio observations (2.3×10^{28}), and the production rate of optical CN using

the theoretical lifetime ($(2.1–2.4) \times 10^{28}$), we conclude that the production rates of the two species are approximately equal. This implies that HCN is the primary parent of CN. However, if the scalelength issue cannot be resolved by better modeling, there is enough uncertainty in the lifetime of CN to allow room for the possibility of a substantial second parent.

4. CONCLUSIONS

Our data show that the jet morphology of HCN and CN are consistent with the CN in jets having an HCN parent. However, the correlation is not strong enough to rule out the possibility of a second parent such as small dust or CHON particles for the CN in jets as was suggested in the P/Halley jets by Klavetter and A'Hearn (1994).

There is an apparent inconsistency between the destruction scalelength of HCN and the formation scalelength of CN which cannot be resolved with the current models. It appears that the HCN scalelength is much longer than the parent scalelength for CN, but without a model that correctly accounts for collisions and acceleration of the gas we cannot be certain of what the true scalelengths are.

The observed production rates in C/Hale–Bopp are, however, consistent with HCN being the dominant parent of CN. There is no doubt that HCN is a primary parent of CN. Is there another contributor that plays as important, or nearly as important, a role? The uncertainty in the CN lifetime, the uncertainty in the scalelengths of HCN and the CN parent, and the possibility of a second parent for the jets leave this an open question.

ACKNOWLEDGMENTS

We thank Amy Lovell for her insightful discussions on HCN and Michel Festou for discussing his results before publication. We also thank Jacques Crovisier for his helpful comments. This work was partially funded by NASA NAG5-4292, NAG5-4080, NAG5-8708, NAG5-8521, NAG5-10491, and NGT5-0083; NSF AST96-13998, AST96-13999, AST96-13716, AST96-15608, AST-21795 and AST99-81363; Taiwanese grants NSC 86-2112-M-003-T and 89-2112-M-003-004; and the Universities of Illinois, Maryland, and California at Berkeley.

REFERENCES

A'Hearn, M. F., S. Hoban, P. V. Birch, C. Bowers, R. Martin, and D. A. Klinglesmith III 1986. Cyanogen jets in Comet Halley. *Nature* **324**, 649–651.

A'Hearn, M. F., R. L. Millis, D. G. Schleicher, D. J. Osip, and P. V. Birch 1995. The ensemble properties of comets: Results from narrowband photometry of 85 comets, 1976–1992. *Icarus* **118**, 223–270.

Biver, N., and 20 colleagues 1997. Long term evolution of the outgassing of Comet Hale–Bopp from radio observations. *Earth, Moon, Planets,* **78**, 5–11.

Bockelée-Morvan, D., and J. Crovisier 1985. Possible parents for the cometary CN radical: Photochemistry and excitation conditions. *Astron. Astrophys.* **151**, 90–100.

Bockelée-Morvan, D., J. Crovisier, A. Baudry, D. Despois, M. Perault, W. M. Irvine, F. P. Schleorb, and D. Swade 1984. Hydrogen cyanide in comets: Excitation conditions and radio observations of Comet IRAS-Aracki-Alcock 1983d. *Astron. Astrophys.* **141**, 411–418.

Bockelée-Morvan, D., J. Crovisier, D. Despois, T. Forveille, E. Gérard, J. Schraml, and C. Thum 1987. Molecular observations of Comets P/Giocabini-Zinner 1984e and P/Halley 1982i at millimetre wavelengths. *Astron. Astrophys.* **180**, 253–262.

Bockelée-Morvan, D., and 17 colleagues 2000. New molecules found in Comet C/1995 O1 (Hale–Bopp). *Astron. Astrophys.* **353**, 1101–1114.

Boehnhardt, H., and K. Birkle 1994. Time variable coma structures in Comet P/Swift–Tuttle. *Astron. Astrophys.* **107**, 101–120.

Combi, M. R. 1987. Sources of cometary radicals and their jets: Gases or grains. *Icarus* **71**, 178–191.

Combi, M. R., and A. H. Delsemme 1980a. Neutral cometary atmospheres I. An average random walk model for photodissociation in comets. *Astrophys. J.* **237**, 633–640.

Combi, M. R., and A. H. Delsemme 1980b. Neutral cometary atmospheres II. The production of CN in comets. *Astrophys. J.* **237**, 641–645.

Combi, M. R., K. Kabin, D. L. DeZeeuw, and T. I. Gombosi 1997. Dust–gas interrelations in comets: Observations and theory. *Earth, Moon, Planets* **79**, 275–306.

Crovisier, J. 1994. Photodestruction rates for cometary parent molecules. *J. Geophys. Res. (Planets)* **99**(E2), 3777–3781.

Crovisier, J., D. Bockelée-Morvan, P. Colom, D. Despois, and G. Paubert 1993. A search for parent molecules at millimetre wavelengths in Comets Austin 1990 V and Levy 1990 XX—Upper limits for undetected species. *Astron. Astrophys.* **269**, 527–540.

de Pater, I., and R. J. Sault 1998. An intercomparison of three-dimensional reconstruction techniques using data and models of Jupiter's synchrotron radiation. *J. Geophys. Res.* **103**(E9), 19973–19984.

Despois, D., J. Crovisier, D. Bockelée-Morvan, J. Schraml, T. Forveille, and E. Gérard 1986. Observations of hydrogen cyanide in Comet Halley. *Astron. Astrophys.* **160**, L11–12.

Dulk, G. A., Y. Leblanc, R. J. Sault, H. P. Ladreiter, and J. E. P. Connerney 1997. The radiation belts of Jupiter at 13 and 22 cm. II. The asymmetries and the magnetic field. *Astron. Astrophys.* **319**, 282–289.

Farnham, T. L., D. G. Schleicher, E. Ford, and E. A. Blount 1997. The rotation period of Hale–Bopp. *Bull. Am. Astron. Soc.* **29**(3), 1033.

Farnham, T. L., D. G. Schleicher, and M. F. A'Hearn 2000. The HB narrowband comet filters: Standard stars and calibrations. *Icarus* **147**, 180–204.

Festou, M. C. 1981. The density distribution of neutral compounds in cometary atmospheres. *Astron. Astrophys.* **95**, 69–79.

Festou, M. C., O. Barale, T. Davidge, S. A. Stern, G. P. Tozzi, M. Womack, and J. M. Zucconi 1998. Tentative identification of the parent of CN radicals in comets: $=C_2N_2$. *Bull. Am. Astron. Soc.* **30**, 1089.

Haser, L. 1957. Distribution d'intensite dans la tete d'une comete. *Bull. Acad. R. Sci. Liege* **43**, 740–750.

Huebner, W. F., L. E. Snyder, and D. Buhl 1974. HCN radio emission from Comet Kohoutek (1973f). *Icarus* **23**, 580–584.

Huebner, W. F., J. J. Keady, and S. P. Lyon 1992. *Solar Photo Rates for Planetary Atmospheres and Atmospheric Pollutants*. Kluwer Academic, Dordrecht.

Irvine, W. M., J. E. Dickens, A. J. Lovell, F. P. Schloerb, M. Senay, E. A. Bergin, D. Jewitt, and H. E. Matthews 1998. Chemistry in cometary comae. *Faraday Discuss.* **109**, 475–492.

Jorda, L., K. Rembor, J. Lecacheux, P. Colom, F. Colas, E. Frappa, and L. M. Lara 1997. The rotational parameters of Hale–Bopp (C/1995 O1) from observations of the dust jets at Pic du Midi Observatory. *Earth, Moon, Planets* **77**, 167–180.

Kissel, J., and 22 colleagues 1986a. Composition of Comet Halley dust particles from Vega observations. *Nature* **321**, 280–282.

Kissel, J., and 18 colleagues 1986b. Composition of Comet Halley dust particles from Giotto observations. *Nature* **321**, 336–337.

Klavetter, J. J., and M. F. A'Hearn 1994. An extended source for CN jets in Comet P/Halley. *Icarus* **107**, 322–334.

Licandro, J., L. R. Bellot Rubio, R. Casas, A. Gómez, M. R. Kidger, N. Sabalisk, P. Santos-Sanz, M. Serra-Ricart, R. Torres-Chico, A. Oscoz, L. Jorda, and G. Denicolo 1997. The spin axis position of C/1995 O1 (Hale–Bopp). *Earth, Moon, Planets* **77**, 199–206.

Licandro, J., L. R. Bellot Rubio, H. Boehnhardt, R. Casas, B. Goetz, A. Gómez, L. Jorda, M. R. Kidger, D. Osip, N. Sabalisk, P. Santos-Sanz, M. Serra-Ricart, G. P. Tozzi, and R. West 1998. The rotation period of C/1995 O1 (Hale–Bopp). *Astrophys. J.* **501**, L221–225.

Lovell, A. J. 1999. *Millimeter-Wave Molecular Mapping of Comets Hyakutake and Hale–Bopp*. Ph.D. thesis, University of Massachusetts.

Magee-Sauer, M., M. J. Mumma, M. A. DiSanti, N. Dello Russo, and T. W. Rettig 1999. Infrared spectroscopy of the ν_3 band of hydrogen cyanide in Comet C/1995 O1 Hale–Bopp. *Icarus* **142**, 498–508.

Newburn, R. L., Jr., and H. Spinrad 1984. Spectrophotometry of 17 comets I. The emission features. *Astron. J.* **89**, 289.

Newburn, R. L., Jr., and H. Spinrad 1989. Spectrophotometry of 25 comets: Post-Halley updates for 17 comets plus new observations for eight additional comets. *Astron. J.* **97**, 552–569.

Randall, C. E., D. G. Schleicher, R. G. Ballou, and D. J. Osip 1992. Observational constraints on molecular scalelengths and lifetimes in comets. *Bull. Am. Astron. Soc.* **24**, 1002.

Rodgers, S. D., and S. B. Charnley 1998. HNC and HCN in comets. *Astrophys. J.* **501**, L227–230.

Samarasinha, N. H. 2000. The coma morphology due to an extended active region and the implications for the spin state of Comet Hale–Bopp. *Astrophys. J.* **529**, L107–110.

Samarasinha, N. H., B. E. A. Mueller, and M. J. S. Belton 1997. Coma morphology and constraints on the rotation of Comet Hale–Bopp (C/1995 O1). *Earth, Moon, Planets* **77**, 189–198.

Sault, R. J., P. J. Teuben, and M. C. H. Wright 1995. A retrospective view of Miriad. In *Astronomical Data Analysis Software and Systems IV* (R. A. Shaw, H. E. Payne, and J. J. E. Hayes, Eds.), Asron. Soc. Pacific Conf. Ser., Vol. 77, pp. 433–436. Astronomical Society of the Pacific, San Francisco.

Schleicher, D. G., T. L. Farnham, W. R. Williams, B. R. Smith, and C. C. Cheung 1999. Modeling the rotational morphology of gas and dust jets in Comet Hale–Bopp (1995 O1) at perihelion. *Bull. Am. Astron. Soc.* **31**(4), 1128.

Schloerb, F. P., W. M. Kinzel, D. A. Swade, and W. M. Irvine 1986. HCN production rates from Comet Halley. *Astrophys. J.* **310**, L55–60.

Schloerb, F. P., W. M. Kinzel, D. A. Swade, and W. M. Irvine 1987. Observations of HCN in Comet P/Halley. *Astron. Astrophys.* **187**, 475–480.

Snyder, L. E., J. M. Veal, L. M. Woodney, M. C. H. Wright, P. Palmer, M. F. A'Hearn, Y.-J. Kuan, I. de Pater, and J. R. Forster 2001. BIMA array photodissociation measurements of HCN and CS in Hale–Bopp (C/1995 O1). *Astron. J.* **121**, 1147–1154.

Veal, J. M., L. E. Snyder, M. C. H. Wright, L. M. Woodney, P. Palmer, J. R. Forster, I. de Pater, M. F. A'Hearn, and Y.-J. Kuan 2000. An interferometric study of HCN in Comet Hale–Bopp (C/1995 O1). *Astron. J.* **119**, 1498.

Winnberg, A., L. Ekelund, and A. Ekelund 1987. Detection of HCN in Comet P/Halley. *Astron. Astrophys.* **172**, 335–341.

Wright, M. C. H., I. de Pater, J. R. Forster, P. Palmer, L. E. Snyder, J. M. Veal, M. F. A'Hearn, L. M. Woodney, W. M. Jackson, Y.-J. Kuan, and A. J. Lovell 1998. Mosaicked images and spectra of $J = 1 \rightarrow 0$ HCN and HCO^+ emission from Comet Hale–Bopp (1995 O1). *Astron. J.* **116**, 3018–3028.

Ziurys, L. M., C. Savage, M. A. Brewster, A. J. Apponi, T. C. Pesh, and S. Wyckoff 1999. Cyanide chemistry in Comet Hale–Bopp (C/1995 O1). *Astrophys. J.* **527**, L67–71.